Key Parameters for Scaling up the Synthesis of Magnetite Nanoparticles in Organic Media: Stirring Rate and Growth Kinetic

ARTICLE *in* INDUSTRIAL & ENGINEERING CHEMISTRY RESEARCH · DECEMBER 2013

Impact Factor: 2.59 · DOI: 10.1021/ie403250p

5 AUTHORS, INCLUDING:

R. Fuentes-Ramirez
Universidad de Guanajuato
31 PUBLICATIONS **118** CITATIONS
SEE PROFILE

Alejandro G. Roca
Catalan Institute of Nanoscience and Nanot…
46 PUBLICATIONS **1,542** CITATIONS
SEE PROFILE

Maria del Puerto Morales
Instituto de Ciencia de Materiales de Madrid
254 PUBLICATIONS **8,008** CITATIONS
SEE PROFILE

I&EC research
Industrial & Engineering Chemistry Research

Article

pubs.acs.org/IECR

Key Parameters for Scaling up the Synthesis of Magnetite Nanoparticles in Organic Media: Stirring Rate and Growth Kinetic

José J. Ibarra-Sánchez,[†] Rosalba Fuentes-Ramírez,[†] Alejandro G. Roca,[§,‡] Maria Del Puerto Morales,[§] and Lourdes I. Cabrera-Lara*[,§,¶]

[†]Universidad de Guanajuato, Campus Guanajuato, Departamento de Ingeniería Química, División de Ciencias Naturales y Exactas, Noria Alta s/n, 36050 Guanajuato, Mexico

[‡]Department of Physics, The University of York, York YO10 5DD, United Kingdom

[§]Instituto de Ciencia de Materiales de Madrid, CSIC, Sor Juana Inés de la Cruz 3, Cantoblanco, 28049 Madrid, Spain

ABSTRACT: The synthesis of magnetic nanoparticles by thermal decomposition in organic media has been studied in this work. The analysis was focused on external parameters, like stirring rate and reaction growth kinetics, given that they are crucial for scaling up the synthesis of magnetic nanoparticles. These parameters have been shown to control magnetite nanoparticle size and size distribution. Magnetite nanoparticles were prepared by thermal decomposition of iron(III) acetylacetonate in 1-octadecene using different stirring rates. At 100 rpm, the largest particle size was achieved, ca. 10 nm, which showed superparamagnetic behavior at room temperature. Growth kinetics were studied at a stirring rate (r) of 100 rpm. Data showed that during magnetite synthesis, particle growth exhibits a sigmoidal behavior and a final Oswald ripening process. Data were fitted to the double Boltzmann function.

1. INTRODUCTION

Magnetic nanoparticles (MNPs) have received great attention worldwide in the last decades because of their possible applications in biomedicine, such as T2 contrast agents in NMR imaging[1] and nanoheaters in hyperthermia.[2] Hence, different groups have developed several synthetic methods for the preparation of these nanoparticles (NPs).[3]

Thermal decomposition of an iron precursor in organic solvents containing surfactants at high temperature,[4] provides better control over size, shape, composition, and internal structure of the MNPs with respect to other methods, such as coprecipitation.[5] However, thermal decomposition is highly sensitive to changes in material balance and operational changes during the reaction, where factors such as the Fe:surfactant:solvent ratio and stirring rate are degrees of freedom that establish the conditions for nanoparticle size control.[6−10]

Variation in particle size as a function of the amount of precursor has been analyzed in 2006 by Casula et al.[11] The study showed that higher amounts of $Fe(CO)_5$ in the reaction mixture increases the system's saturation, forming many nuclei. Hence, a small amount of the precursor species remains to promote particle growth, leading to the generation of particles of small size (4 nm). However, when $Fe(acac)_3$ is used as precursor and its concentration is doubled, particles grow up to 8 nm in diameter.[9] In 2001, Hyeon et al.[10] analyzed the effect of the Fe:oleic acid (OA) ratio in the synthesis of γ-Fe_2O_3 NPs using $Fe(CO)_5$ as precursor. Results showed that particles of 4, 7, and 11 nm were generated when the Fe:oleaic acid ratio was 1:1, 1:2, and 1:4, respectively. There are two other variables widely used to control the size of NPs produced by thermal decomposition: solvent and surfactant. In thermal decomposition, the extended temperature range enables iron organic precursors to decompose.[12] Hence, when a solvent with a higher boiling point is used, particle size increases.[7,13] By controlling the amount and nature of the surfactant, the final particle size varies opposite the binding force between Fe atoms and the functional group present at the surfactant.[8] Moreover, the binding strength determines the decomposition temperature of the precursor, leading to free species that subsequently give rise to nuclei that diffuse to the surface of particles in the growth stage.

Therefore, the production of these NPs with a specific size requires the control of many different synthesis parameters, such as the type of precursor, surfactant, and solvent as well as the Fe:surfactant:solvent ratio. In addition to these, when performing a large scale reaction, variables such as stirring rate, stirring period, reaction temperature, and reaction time need to be taken into account to yield uniform, homogeneous, and disperse MNPs.

For example, tuning the stirring rate during the synthesis of Cu_2O, NPs can be shaped from flakes to cubes.[14] During the synthesis of iron oxide NPs, magnetic properties can also be affected[15] because particle size and Fe:O ratio can change by tuning the stirring rate.[15,16] Several studies have been made about this aspect. Stirring rate has been evaluated in order to understand its effect in the synthesis of NPs generated by several methods. In general, the effect is observed in the NPs morphology,[14] particle size,[17−21] and particle size distribution.[21−24] Most of the studies performed for the synthesis of MNPs have been carried out using the coprecipitation method. Researchers agree that as stirring rate increases (r = 300−1500 rpm), mobility and homogeneous distribution of the Fe_3O_4

Received: June 14, 2013
Revised: November 10, 2013
Accepted: November 19, 2013

   dx.doi.org/10.1021/ie403250p | Ind. Eng. Chem. Res. XXXX, XXX, XXX−XXX

species also increase, generating smaller and more narrowly size-distributed particles.[15,24−30] Sun et al.[26] explained that this is due to the increase of the energy transferred to the suspension medium. The reaction solution can be dispersed into smaller droplets, and the size is reduced. Another explanation was given by Hua et al.,[27] who state that this reduction is due to the anomalous diffusion of particles at higher degree of agitation, which reduced the growth kinetics of the particles, resulting in smaller particles. Following this technique, Lin et al.[25] were able to obtain Fe_3O_4 NPs of different diameters resulting from diverse stirring rates (r = 300 rpm and d = 13.1 ± 2.1 nm, r = 600 rpm and d = 9.2 ± 1.1 nm, and r = 900 rpm and d = 6.7 ± 1.3 nm). Mahmoudi et al.[31,32] generated superamagnetic magnetite NPs coated with polyvinyl alcohol as well, following the same synthetic method, and found that stirring rate also affects the nanoparticle morphology and, hence, its importance on mass transfer and crystal growth rate.

However, most of these studies have been carried out at relatively low temperatures (T = 80 °C) and at very high stirring rates, which are placed between 100 and 12 500 rpm. The present work aims to study the effect of low stirring rates (r = 0−240 rpm) on particle size and size distribution and shed some light on the growth kinetic of magnetite NPs synthesized by thermal decomposition (T = 240−300 °C) of organic precursors in organic media. These variables at an industrial production level can be controlled and could be used to generate the desired particle size for a specific application. It is well known that uniform and well-defined NPs are required for biomedical applications to avoid the use of large doses or the manifestation of secondary effects after intravenous injection.[33]

2. MATERIAL AND METHODS

2.1. Preparation of Magnetite MNPs. Magnetite NPs were prepared by thermal decomposition of $Fe(acac)_3$ in 1-octadecene in the presence of oleic acid (OA) and oleylamine (ODA). $Fe(acac)_3$ (20 mmol), 100 mmol of 1,2-dodecanediol, 60 mmol of OA, 60 mmol of ODA, and 200 mL of 1-octadecene were added to a spherical flask. The mixture was mechanically stirred for 5 min at room temperature and then heated up to 200 °C under an N_2 gas flow. The reaction was kept at this temperature for 2 h before N_2 flow was removed and the reaction was heated up to reflux for 30 min. The synthesis was carried out at the following mechanical stirring rates: 0.0 (M1), 33 (M2), 100 (M3), 170 (M4), and 240 (M5) rpm.

Particles were washed by mixing the particle suspension with the same volume of ethanol and centrifuged for 10 min at 420 rpm. Then, supernatant was discarded, and the precipitate was redispersed in hexane. This process was repeated until the supernatant became transparent. Powder was achieved after drying the precipitate that contained the NPs with nitrogen.

2.2. Growth Kinetic Analysis of MNPs. The study of particle growth during synthesis was carried out for r = 100 rpm, keeping the other parameters the same as described above. The kinetic study was conducted by taking a 1 mL aliquot every 30 min during the stabilization state, with T = 200 °C as previously described, until the reaction ended.

2.3. Characterization. The aggregate size of the particles was acquired with a Dynamic Light scattering (DLS) (ZETASIZER NANO ZS, Malvern Instruments). Phase and crystal size of the iron oxide particles was identified by powder X-ray diffraction (XRD). The X-ray patterns were performed with a Baker model X'PERT of PANalytical with Cu Kα radiation (1.5406 Å). Particle size and morphology were studied by transmission electronic microscopy (TEM) using a 200 keV JEOL-2000 FXII microscope. Mean particle size (D_{TEM}) and size distribution were evaluated by measuring the largest internal dimension of at least 300 particles. Particle size distribution was fitted afterward to a log-normal function.

Magnetic characterization of the samples was carried out in a vibrating sample magnetometer (MLVSM9Maglab 9 T, Oxford Instruments) at room temperature. Saturation magnetization (M_s) was evaluated by plotting M versus $1/H$ at high fields. M_s values were corrected from the organic content that was determined by thermogravimetric analysis. The viscosity of all samples was measured at 23 °C using a Cannon-Fenske viscometer, Comect brand. Three readings of each sample were taken to ensure the reproducibility of results.

3. RESULTS AND DISCUSSION

3.1. MNPs Nature. Generated iron oxide NPs by thermal decomposition were characterized. As stated in the previous section, OA and ODA were employed in order to act as stabilizers and reducing agents. Figure 1 shows the DLS size

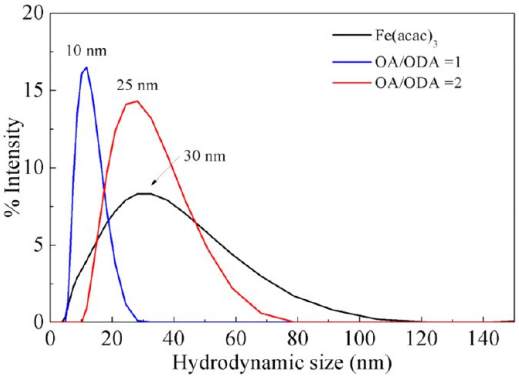

Figure 1. Hydrodynamic size measured by DLS of Fe_3O_4 NPs suspension in organic media synthesized without surfactant and with different OA:ODA ratios.

distribution of iron oxide NPs generated without the presence of OA/ODA and in the presence of different amounts of OA and ODA. It can be noticed that the presence of OA and ODA dramatically improved the size distribution of the final particles, being narrower for OA:ODA 1:1 ratio. The OA:ODA ratio provided a good control over crystallization, size, and morphology. The coordination of the OA to iron oxide nanoparticle's surface was stronger than ODA. Usually in the presence of ODA, MNPs are bigger and particle size distribution is wider. A compromise had to be attained between size and distribution, which is why, in our case, we used a 1:1 ratio.[34−36]

Figure 2 shows the different XRD patterns for MNPs synthesized by thermal decomposition at different stirring rates. Data show that final products presented similar patterns, which correspond to an inverse spinel structure. This structure is characteristic of magnetite (Fe_3O_4) NPs (JCPDS no. 19-0629).

No extra peaks due to secondary phases were observed in any of the samples as expected and reported before.[2] The small deviation present in all cases could be due to defects inherent to the material in its nanocrystalline structure, mainly surface defects.[37] Additionally, a slight oxidation to maghemite could also contribute to such defects.[38]

dx.doi.org/10.1021/ie403250p | Ind. Eng. Chem. Res. XXXX, XXX, XXX−XXX

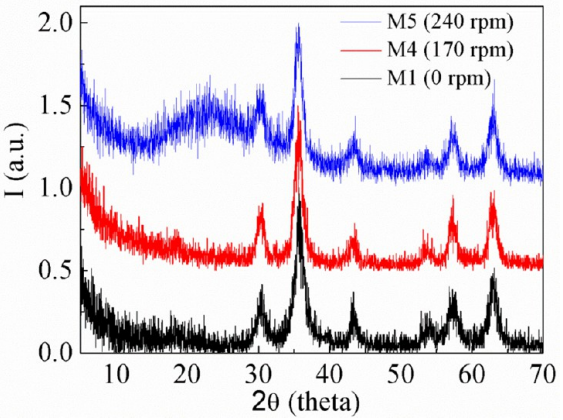

Figure 2. XRD pattern of MNPs samples synthesized at different stirring rates: M1 (r = 0 rpm), M4 (r = 170 rpm), and M5 (r = 240 rpm).

By using the Scherrer equation, crystallite sizes for samples M1, M4, and M5 were estimated to be 5.8, 8.0, and 7.1 nm respectively. For each case, the lattice parameter was calculated (a_0) and the results are shown in Table 1.

Figure 3 shows the TEM images of particles synthesized at different stirring rates. Micrographs show that the final particle size increases from 7.7 nm (r = 0 rpm) to 10.5 nm at 100 rpm.

The use of higher stirring rates led to a particle size decrease down to 7.8 nm. Crystal size calculated from the Scherrer equation and particle size from TEM measurements were similar, and the slight difference between these values could be due to surface effects (lower crystallinity at the particle surface).[39]

Figure 4 shows the hysteresis loops for M1, M2, M3, M4, and M5 measured at room temperature. All MNPs samples exhibited superparamagnetic behavior at room temperature, which is typical of magnetite nanoparticles of sizes less than or equal to 10 nm.[6] As it can be observed, M_s values increased from 69 up to 76 emu/g as the stirring rate increased from 0 to 170 rpm. Particle size and the possible content of a magnetite core in some particles prepared at higher stirring rate could account for a higher saturation magnetization.

The calculated values of M_s for all magnetite samples (Table 1) were close to the M_s value reported for magnetite nanoparticles prepared by a similar method, and they were smaller than the value reported for bulk material (84 emu/g).[40] Samples M4 and M5, generated at higher stirring rates, presented higher M_s values, suggesting an improvement in OA molecules' bonding. This allowed a better dispersion of the particles.[41]

3.2. Effect of Stirring Rate. Figure 5 shows a graphic representation of the effect of stirring rate. It can be inferred that at slow rates (0 < r < 100 rpm), particle size increases, reaching a maximum value at 100 rpm. However, at higher rates, particle size decreases as observed by TEM (Figure 5 and Table 1). The same behavior is observed in the polydispersity of mean size values (broadening the size distribution). Both cases can be explained by transport phenomena, where mass transport (or mixing) results from diffusion, convection, or both.[42]

Crystal growth from solution is a very complicated process that involves several steps.[43] In this case, when keeping constant supersaturation conditions, the growth rate seems to be limited by the rate of mass transport of new material to the crystal surface. Below 100 rpm, diffusion dominates the reaction. This means that mass transport occurs without requiring bulk motion. Mass transfer is limited so the formation of a small number of nuclei takes place at the beginning of the reaction, promoting MPNs growth. At 100 rpm, phenomenon of diffusion combined with the phenomenon of convection (motion of the reaction solution) promotes a better mass transfer in the reaction solution, allowing particle growth. For stirring rates greater than 100 rpm, convection dominates and nucleation is favored due to the increase in mass transfer, so growth is limited. This observation indicates that polydispersity is a result of convection and diffusion (r = 100 rpm) activated at the same time. Similar results were published by Karaagac et al.[15] They found that for superparamagnetic iron oxide NPs prepared by coprecipitation, when increasing stirring rates from 300 to 1800 rpm, particle size first increased from 12 nm (r = 300 rpm) to 13.5 nm (r = 1100 rpm) and then dropped to 7 nm at r = 1800 rpm. Khan et al.[16] also reported that the Fe:O ratio decreased with stirring rate, along with particle size (r = 600−1100 rpm gives magnetite NPs of 12 and 8 nm, respectively).

This also explains the difference in crystallite size observed when calculating NP size by Scherrer's equation (Table 1). At stirring rates higher than 100 rpm, OA and ODA are more available to the nuclei. It should be taken into account that OA and ODA act as particle size stabilizers, occupying active sites at the NP surface. The diffusion of iron ions to the active sites is hindered by these inhibitor molecules, and the grain growth is disturbed. For this reason, the crystallite size decreases.[44]

Stirring rate also has an effect on the viscosity of the reactor's effluent. With Newtonian fluids (typically water and solutions containing only low molecular weight material) viscosity is independent of shear strain rate, and a plot of shear strain rate (e.g., stirring rate) against shear stress[45] (for example, force per unit area stirred required for stirring) is linear and passes through the origin. However, this is not the case in this study. For this reason, it was of interest to relate viscosity with stirring rate and MNPs final size (Figure 6). As it can be observed, viscosity of the effluent from the reactor is inversely

Table 1. Physical Properties of MNPs Samples[a]

sample	stirring rate (rpm)	D_{TEM} (nm)	S.D. (nm)	log σ	D_{XRD} (nm)	a_0 (nm)	M_S (emu/g)	% coating	η (cP)
M1	0	7.7	1.3	0.13	5.8	0.8394	69	26.3	13.3
M2	33	9.3	1.4	0.15			68	13.4	8.5
M3	100	10.2	1.5	0.17			70	23.9	5.7
M4	170	8.4	1.3	0.13	8.0	0.8395	77	19.9	18.6
M5	240	7.8	1.4	0.14	7.1	0.8395	76	16.9	15.8

[a]Particle size, D_{TEM}; standard deviation, S.D.; polydispersity, log σ; crystallite size, D_{XRD}; lattice parameter, a_0; saturation magnetization, M_s; percentage of OA coating the nanoparticle's surface, % coating; viscosity, η.

dx.doi.org/10.1021/ie403250p | Ind. Eng. Chem. Res. XXXX, XXX, XXX−XXX

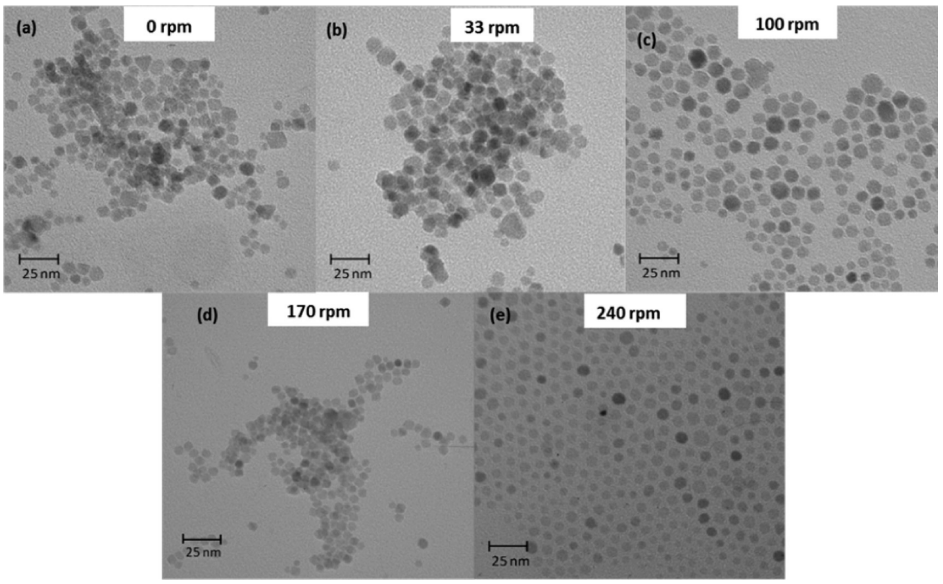

Figure 3. TEM micrographs of magnetite samples (a) M1, (b) M2, (c) M3, (d) M4, and (e) M5.

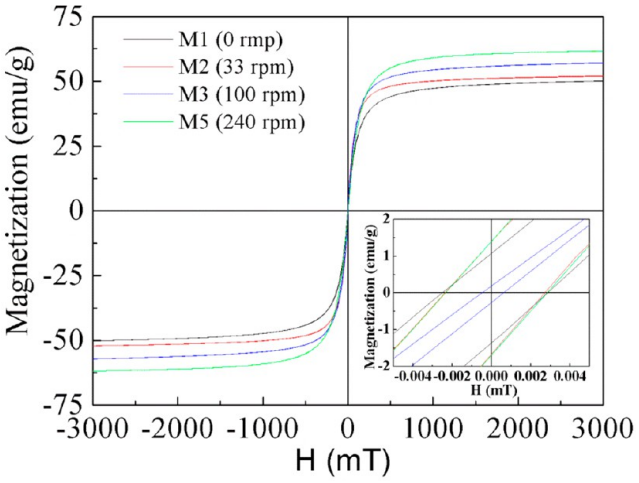

Figure 4. Room temperature hysteresis loops of MNPs samples M1, M2, M3, and M5, synthesized at different stirring rates.

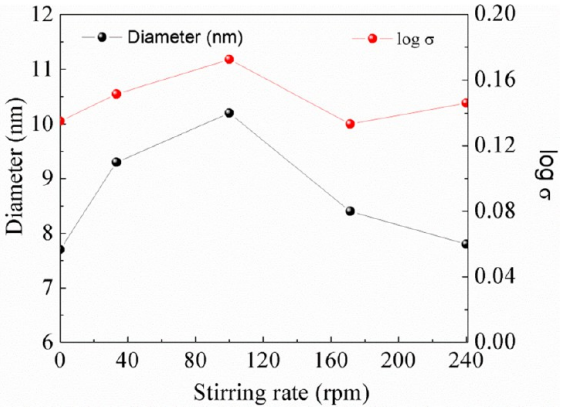

Figure 5. Diameter and polydispersity of MNPs as a function of stirring rate.

proportional to magnetite particle size. For less than or equal to r = 100 rpm, particle size is high and viscosity is low. The contrary case is observed for rates higher than 100 rpm. This

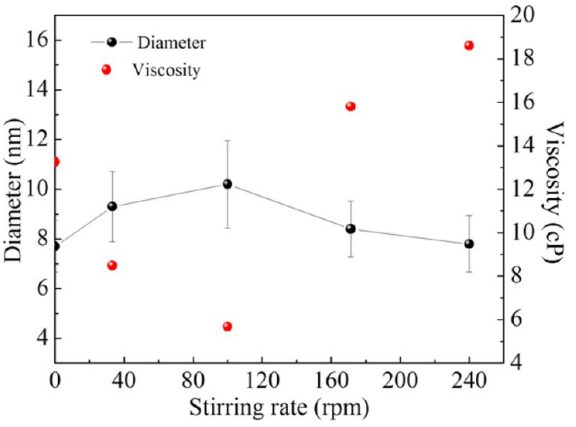

Figure 6. Particle diameter and viscosity of the effluent at T = 23 °C as a function of stirring rate.

inverse correlation revealed that at for $r \leq 100$ rpm, iron precursor and stabilizing surfactant have been consumed, whereas for $r > 100$ rpm, great amounts of precursor and surfactant are still present and do not react. This is of great interest because it is an indication of the best conditions at which the reaction reaches completion.

3.3. Growth Kinetics Study. To understand the kinetics of the magnetite NPs reaction produced by thermal decomposition, a stirring rate of r = 100 rpm during the stabilization stage (T = 200 °C) was selected because particles show narrow size distribution and homogeneous morphology.

There are three regimes of particle size generation: induction time, nucleation period, and growth stage. During the reaction, the generated nucleus have to reach a certain critical radius, after which it becomes stable and then undergoes subsequent growth. Particles with a radius smaller than the critical radius dissolve into the reaction medium. If the stirring rate is slow, the yield of particles is low.[43,46] Due to these observations at slow rates, this study focuses on a stirring rate of r = 100 rpm.

TEM micrographs were taken for different reaction times, 120, 150, 180, 194, 204, and 214 min (Figure 7), and particle size was measured. It is observed that at this stage, polydispersity decreased (Figure 7).

dx.doi.org/10.1021/ie403250p | Ind. Eng. Chem. Res. XXXX, XXX, XXX−XXX

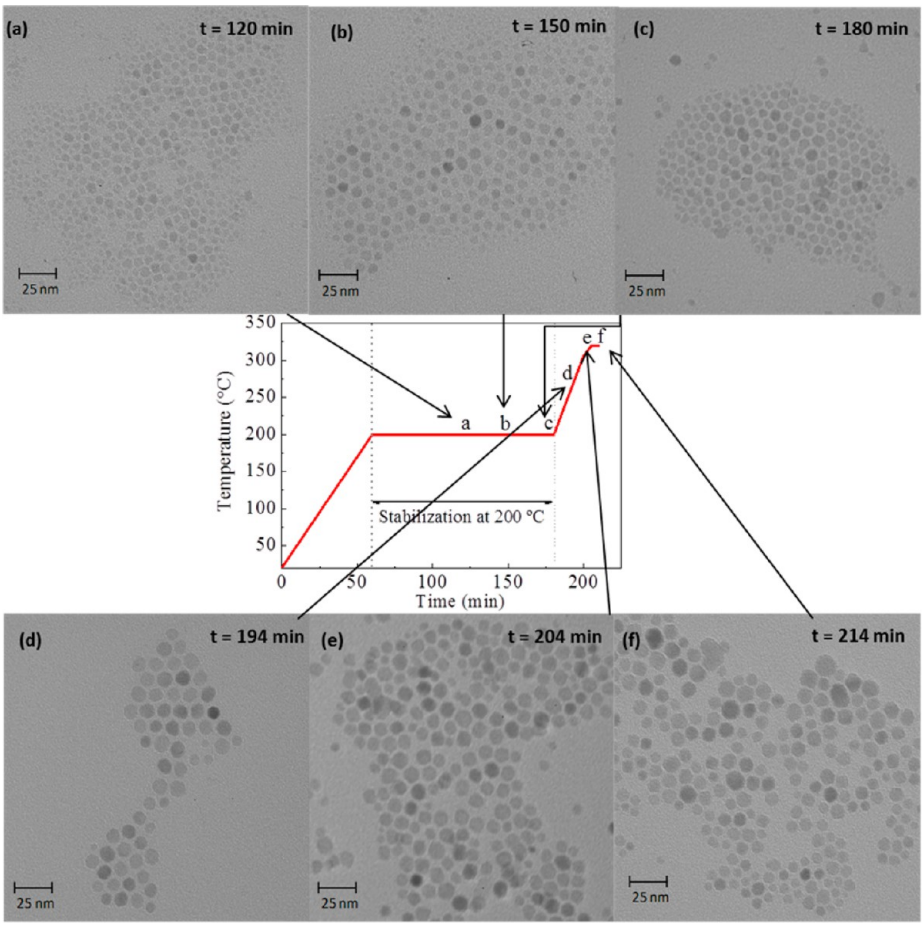

Figure 7. TEM micrographs of MNPs generated at r = 100 rpm at different reaction times: (a) 120, (b) 150, (c) 180, (d) 194, (e) 204, and (f) 214 min.

During the formation of intermediate species, some newly formed nuclei begin to grow at the expense of the intermediate species; that is, it is a premature growth. However, the production of precursor species is faster; thus, that growth eventually becomes homogeneous. As a result, the polydispersity of the sample decreases, becoming almost constant throughout the reaction (Table 2).

Table 2. Structural Characterization of Particles Formed at Different Reaction Times[a]

time (min)	D_{TEM} (nm)	S.D. (nm)	log (σ)	temperature (°C)
90	2.6	1.7	0.24	200
120	5.3	1.5	0.17	200
150	6.7	1.3	0.13	200
180	6.9	1.5	0.17	200
194	8.6	1.4	0.14	311
204	8.9	1.4	0.14	318
214	10.2	1.5	0.17	318

[a]Particle size, D_{TEM}; standard deviation, S.D.; polydispersity, log σ.

Figure 8 shows the representation of particle growth as a function of reaction time. This behavior follows a sigmoidal shape (logistics). It can be observed that the sigmoid curve has two sections: the first section is characterized by fast particle growth (90 < t < 150 min), becoming asymptotic at a particle size of 7 nm at 130 min. This rapid increase in size can be related to the clustering of most of the intermediate species

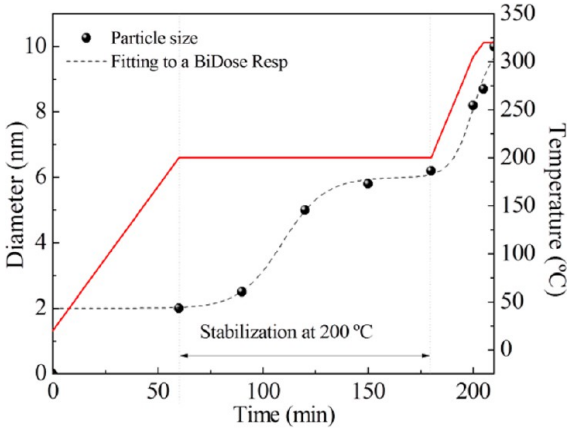

Figure 8. Particle size and reaction temperature as a function of reaction time for the synthesis carried out at r = 100 rpm.

formed at low temperature to form nuclei that will generate the first particles. After the reaction mixture is depleted of intermediate species, diffusion of the remaining intermediate species is not favored because of the low temperature with respect to the solvent's boiling point.

In the second section of the curve, which represents the final growth, once the temperature increased again, particle growth is favored. Finally, the curve becomes asymptotic because the reaction mixture no longer has intermediate species to allow additional growth. This observation agrees with our assump-

dx.doi.org/10.1021/ie403250p | Ind. Eng. Chem. Res. XXXX, XXX, XXX−XXX

tion, validating what we have exposed. Because these two stages (nucleation and growth) integrated a rapid growth and an asymptote, we fitted the data to the double Boltzmann function.[47]

$$D_{TEM} = A_1 + (A_2 - A_1)\left[\frac{p}{1 + 10^{(\log_{x_1} - t)h_1}} + \frac{1 - p}{1 + 10^{(\log_{x_2} - t)h_2}}\right] \quad (1)$$

where A_1, A_2, $\log_{x_1}$, $\log_{x_2}$, p, h_1, and h_2 are constants of the proposed model, t is the reaction time, and D_{TEM} the diameter of the particles. Figure 7 shows the kinetic model fitted to the experimental data for particle growth. A_1 refers to the initial particle size value of the curve (A_1 = 2.6 nm), which in this case can be interpreted as nuclei size at time t_0. The value for h_1 (40.11) refers to the first slope of the curve. As can be observed, the value is very high, which indicates a fast growing stage of particles (burst nucleation). The value for h_2 (0.045) is also given by a slope; however, in this case, it indicates that particle growth takes place at slower rate. Final particle size is given by A_2, which is 10.2 nm.

The kinetic of growth shows a pattern similar to the one presented by bacteria and autocatalytic reactions[48,49] because in both cases, a stage of rapid growth is followed by one of slow growth, repeatedly, until finally it becomes asymptotic. This behavior indicates that Ostwald ripening is taking place at the end of the reaction, helping to obtain uniform particles.[50]

These results show that another important parameter that allows particle size control is the reaction kinetic, which is affected not only by stirring rate, as demonstrated before, but also by temperature gradient and the time used during the reaction.

4. CONCLUSIONS

Operating parameters were analyzed in the synthesis of magnetite NPs by thermal decomposition. In this synthesis route, the stirring speed (r = 100 rpm) determines the maximum size MNPs can reach (ca. 10 nm), and this is key to determining the maximum yield of the reaction. It was concluded that mass transport is governed by convection. The study of the kinetics of growth showed a similar pattern to the one observed for bacteria and autocatalytic reactions because in both cases, there is first a stage of rapid growth, then a stage of slow-growth, followed by another fast-growing stage, with growth finally becoming asymptotic at the end value. This behavior indicates that the particles grow at the expense of other newly formed particles.

AUTHOR INFORMATION

Corresponding Author

*L. I. Cabrera-Lara. E-mail address: lourisa_cabrera@yahoo.com.

Present Address

¶Centro Conjunto de Investigación en Química Sustentable UAEM-UNAM, Km. 14.5 Carretera Toluca-Atlacomulco, 50200 Toluca, Estado de Mexico, Mexico.

Notes

The authors declare no competing financial interest.

ACKNOWLEDGMENTS

This work was partially supported by grants from the Spanish Ministry of Economy and Competitiveness (MAT2011-23641). A.G.R. acknowledges financial support from the Spanish Ministerio de Educación through Programa Nacional de Movilidad de Recursos Humanos of Plan Nacional of I-D+i 2008-2011. We acknowledge Maria Carrillo and MBA Beatriz E. Cabrera and the financial support provided by Universidad de Guanajuato and CONACyT (México).

ABBREVIATIONS

MNPs = magnetic nanoparticles
NPs = nanoparticles
r = stirring rate
acac = acetylacetonate
OA = oleic acid
ODA = oleylamine
rpm = revolutions per minute
DLS = dynamic light scattering
TEM = transmission electronic microscope
XRD = X-ray diffraction
TGA = thermogravimetric analysis
DGA = differential gravimetric analysis
M_s = saturation magnetization
JCPDS = Joint Committee on Powder Diffraction Standards

REFERENCES

(1) Corot, C.; Robert, P.; Idée, J.-M.; Port, M. Recent advances in iron oxide nanocrystal technology for medical imaging. *Adv. Drug Delivery Rev.* **2006**, *58*, 1471−1504.

(2) Rosensweig, R. E. Heating magnetic fluid with alternating magnetic field. *J. Magn. Magn. Mater.* **2002**, *252*, 370−374.

(3) Roca, A. G.; Costo, R.; Rebolledo, A. F.; Veintemillas-Verdaguer, S.; Tartaj, P.; González-Carreño, T.; Morales, M. P.; Serna, C. J. Progress in the preparation of magnetic nanoparticles for applications in biomedicine. *J. Phys. D: Appl. Phys.* **2009**, *42*, 224002−224012.

(4) Rockenberger, J.; Scher, E. C.; Alivisatos, A. P. A New Nonhydrolytic Single-Precursor Approach to Surfactant-Capped Nanocrystals of Transition Metal Oxides. *J. Am. Chem. Soc.* **1999**, *121*, 11595−11596.

(5) Massart, R. Preparation of aqueous magnetic liquids in alkaline and acidic media. *IEEE Trans. Magn.* **1981**, *17*, 1247−1248.

(6) Roca, A. G.; Morales, M. P.; O'Grady, K.; Serna, C. J. Structural and magnetic properties of uniform magnetite nanoparticles prepared by high temperature decomposition of organic precursors. *Nanotechnology* **2006**, *17*, 2783−2788.

(7) Park, J.; An, K.; Hwang, Y.; Park, J.-G.; Noh, H.-J.; Kim, J.-Y.; Park, J.-H.; Hwang, N.-M.; Hyeon, T. Ultra-large-scale syntheses of monodisperse nanocrystals. *Nat. Mater.* **2004**, *3*, 891−895.

(8) Cheon, J.; Kang, N.-J.; Lee, S.-M.; Lee, J.-H.; Yoon, J.-H.; Oh, S. J. Shape Evolution of Single-Crystalline Iron Oxide Nanocrystals. *J. Am. Chem. Soc.* **2004**, *126*, 1950−1951.

(9) Sun, S.; Zeng, H. Size-Controlled Synthesis of Magnetite Nanoparticles. *J. Am. Chem. Soc.* **2002**, *224*, 8204−8205.

(10) Hyeon, T.; Lee, S. S.; Park, J.; Chung, Y.; Na, H. B. Synthesis of Highly Crystalline and Monodisperse Maghemite Nanocrystallites without a Size-Selection Process. *J. Am. Chem. Soc.* **2001**, *123*, 12798−12801.

(11) Casula, M. F.; Jun, Y.-w.; Zaziski, D. J.; Chan, E. M.; Corrias, A.; Alivisatos, A. P. The Concept of Delayed Nucleation in Nanocrystal Growth Demonstrated for the Case of Iron Oxide Nanodisks. *J. Am. Chem. Soc.* **2006**, *128*, 1675−1682.

(12) Peng, S.; Sun, S. Synthesis and characterization of monodisperse hollow Fe3O4 nanoparticles. *Angew. Chem., Int. Ed.* **2007**, *46*, 4155−4158.

(13) Roca, A. G.; Veintemillas-Verdaguer, S.; Port, M.; Robic, C.; Serna, C. J.; Morales, M. P. Effect of Nanoparticle and Aggregate Size on the Relaxometric Properties of MR Contrast Agents Based on High Quality Magnetite Nanoparticles. *J. Phys. Chem. B* **2009**, *113*, 7033−7039.
(14) Bai, Y.; Yang, T.; Gu, Q.; Cheng, G.; Zheng, R. Shape control mechanism of cuprous oxide nanoparticles in aqueous colloidal solutions. *Powder Tech.* **2012**, *227*, 35−42.
(15) Karaagac, O.; Kockar, H. Effect of Synthesis Parameters on the Properties of Superparamagnetic Iron Oxide Nanoparticles. *J. Supercond. Novel Magn.* **2012**, *25*, 2777−2781.
(16) Khan, U. S.; Khattak, N. S.; Rahman, A.; Khan, F. Optimal Method for Preparation of Magnetite Nanoparticles. *J. Chem. Soc. Pak.* **2011**, *33*, 628−633.
(17) Hertz, A.; Drobek, M.; Ruiz, J.-C.; Sarrade, S.; Guizard, C.; Julbe, A. Robust synthesis of yttria stabilized tetragonal zirconia powders (3Y-TZPs) using a semi-continuous process in supercritical CO_2. *Chem. Eng. J.* **2013**, *228*, 622−630.
(18) Schmidt, J.; Guesdon, C.; Schomäcker, R. Engineering aspects of preparation of nanocrystalline particles in microemulsions. *J. Nanopart. Res.* **1999**, *1*, 267−276.
(19) Alveroglu, E.; Yavarinia, N.; Yilmaz, Y. Kinetics of ZnO nanoparticle formation via fluorescence measurements. *J. Lumin.* **2013**, *143*, 741−745.
(20) Kumar, D.; Meenan, B. J.; Mutreja, Isha; D'sa, R.; Dixon, D. Controlling the size and size distribution of gold nanoparticles: A design of expriment study. *Int. J. Nanosci.* **2012**, *11*, 7.
(21) Kim, K. Y.; Choi, Y. T.; Seo, D. J.; Park, S. B. Preparation of silver colloid and enhancement of dispersion stability in organic solvent. *Mater. Chem. Phys.* **2004**, *88*, 377−382.
(22) Salimi, M. N.; Anuar, A. Characterizations of Biocompatible and Bioactive Hydroxyapatite Particles. *Procedia Eng.: Malaysian Technical Universities Conference on Engineering & Technology 2012, MUCET 2012* **2013**, *53*, 192−196.
(23) Salimi, M. N.; Bridson, R. H.; Grover, L. M.; Leeke, G. A. Effect of processing conditions on the formation of hydroxyapatite nanoparticles. *Powder Tech.* **2012**, *218*, 109−118.
(24) Devaraj, N. K.; Ong, B. H.; Matsumoto, M. Characterization of Chemically Prepared Magnetite. *Synth. React. Inorg., Met.−Org., Nano−Met. Chem.* **2008**, *38*, 204−207.
(25) Devaraj, N. K.; Ong, B. H. Effects of Calcination on the Magnetic Properties of Iron Oxide Nanoparticles. *AIP Conf. Proc.* **2011**, *1328*, 288−291.
(26) Devaraj, N. K.; Ong, B. H.; Matsumoto, M. Yield Control of Chemically-Synthesized Magnetite Nanoparticles. *Synth. React. Inorg., Met.−Org., Nano−Met. Chem.* **2008**, *38*, 208−211.
(27) Lin, R.-Y.; Dayananda, K.; Chen, T.-J.; Chen, C.-Y.; Liu, G.-C.; Lin, K.-L.; Wang, Y.-M. Targeted RGD nanoparticles for highly sensitive in vivo integrin receptor imaging. *Contrast Media Mol. Imaging* **2012**, *7*, 7−18.
(28) Sun, J.; Zhou, S.; Hou, P.; Yang, Y.; Weng, J.; Li, X.; Li, M. Synthesis and characterization of biocompatible Fe_3O_4 nanoparticles. *J. Biomed. Mater. Res., Part A* **2007**, *80*, 333−341.
(29) Hua, C. C.; Zakaria, S.; Farahiyan, R.; Khong, L. T.; Nguyen, K. L.; Abdullah, M.; Ahmad, S. Size controlled synthesis and characterization of Fe_3O_4 nanoparticles by chemical coprecipitation method. *Sains Malays.* **2008**, *37*, 389−394.
(30) Mahdavi, M.; Ahmad, M. B.; Haron, M. J.; Namvar, F.; Nadi, B.; Rahman, M. Z. A.; Amin, J. Synthesis, Surface Modification and Characterisation of Biocompatible Magnetic Iron Oxide Nanoparticles for Biomedical Applications. *Molecules* **2013**, *18*, 7533−7548.
(31) Mahmoudi, M.; Simchi, A.; Imani, M.; Milani, A. S.; Stroeve, P. Optimal Design and Characterization of Superparamagnetic Iron Oxide Nanoparticles Coated with Polyvinyl Alcohol for Targeted Delivery and Imaging. *J. Phys. Chem. B* **2008**, *112*, 14470−14481.
(32) Mahmoudi, M.; Shokrgozar, M. A.; Simchi, A.; Imani, M.; Milani, A. S.; Stroeve, P.; Vali, H.; Häfeli, U. O.; Bonakdar, S. Multiphysics Flow Modeling and in Vitro Toxicity of Iron Oxide Nanoparticles Coated with Poly(vinyl alcohol). *J. Phys. Chem. C* **2009**, *113*, 2322−2331.
(33) Bolden, N. W.; Rangari, V. K.; Jeelani, S.; Boyoglu, S.; Singh, S. R. Synthesis and Evaluation of Magnetic Nanoparticles for Biomedical Applications. *J. Nanoparticles* **2013**, *2013*, 370812−9.
(34) Bu, W.; Chen, Z.; Chen, F.; Shi, J. Oleic Acid/Oleylamine Cooperative-Controlled Crystallization Mechanism for Monodisperse Tetragonal Bipyramid $NaLa(MoO_4)_2$ Nanocrystals. *J. Phys. Chem. C* **2009**, *113*, 12176−12185.
(35) Farahmandjou, M. Effect of Oleic Acid and Oleylamine Surfactants on the Size of FePt Nanoparticles. *J. Supercond. Novel Magn.* **2012**, *25*, 2075−2079.
(36) Xu, Z.; Shen, C.; Hou, Y.; Gao, H.; Sun, S. Oleylamine as Both Reducing Agent and Stabilizer in a Facile Synthesis of Magnetite Nanoparticles. *Chem. Mater.* **2009**, *21*, 1778−1780.
(37) Mürbe, J.; Rechtenbach, A.; Töpfer, J. Synthesis and physical characterization of magnetite nanoparticles for biomedical applications. *Mater. Chem. Phys.* **2008**, *110*, 426−433.
(38) Roca, A. G.; Marco, J. F.; Morales, M. d. P.; Serna, C. J. Effect of nature and particle size on properties of uniform magnetite and maghemite nanoparticles. *J. Phy. Chem. C* **2007**, *111*, 18577−18584.
(39) Batlle, X.; Labarta, A. Finite-size effects in fine particles: magnetic and transport properties. *J. Phys. D: Appl. Phys.* **2002**, *35*, R15−R42.
(40) Cullity, B. D. *Introduction to Magnetic Materials*; Addison-Wesley Pub. Co.: Boston, MA, 1972.
(41) Morales, M. A.; Jain, T. K.; Labhasetwar, V.; Leslie-Pelecky, D. L. Magnetic studies of iron oxide nanoparticles coated with oleic acid and Pluronic® block copolymer. *J. Appl. Phys.* **2005**, *97* (10Q905), 1−3.
(42) Goldstein, R. J. *Mass transfer systems for simulating heat transfer processes. Measurement techniques in heat and mass transfer*; Hemisphere Publishing Corp.: Washington, DC, 1985; pp 215−229.
(43) Cornell, R. M.; Schwertmann, U. *The Iron Oxides: Structure, Properties, Reactions, Occurrences and Uses*, 2nd ed.; Wiley-VCH: Weinheim, Germany, 2003; p 703.
(44) Natter, H.; Hempelmann, R. Nanocrystalline Copper by Pulsed Electrodeposition: The Effects of Organic Additives, Bath Temperature, and pH. *J. Phys. Chem.* **1996**, *100*, 19525−19532.
(45) Bird, R. B.; E.Stewai, W.; Lightfoot, E. N. *Transport Phenomena*, 3rd ed.; John Wiley & Sons, Inc.: Hoboken, NJ, 2007; p 905.
(46) Wang, L.; Muhammed, M. Synthesis of Zinc Oxide Nanoparticles with Controlled Morphology. *J. Mater. Chem.* **1999**, *9*, 2871−2878.
(47) Landau, L. D.; Lifshitz, E. M., *Statistical Physics Part 1*, Vol *5*, 3rd ed.; Pergamon Press Ltd.: Oxford, U. K., 1980; p 563.
(48) Bonilla-Petricioleta, A.; Rangaiah, G. P. Evaluation of stochastic global optimization methods for modeling vapor−liquid equilibrium data. *Fluid Phase Equilib.* **2010**, *287*, 111−125.
(49) Perret, C. J. A New Kinetic Model of a Growing Bacterial Population. *J . Gen. Microbiol.* **1960**, *22*, 589−617.
(50) LaMer, V. K.; Dinegar, R. H. Theory, Production and Mechanism of Formation of Monodispersed Hydrosols. *J. Am. Chem. Soc.* **1950**, *72*, 4847−4854.